Cavitation erosion of copper and aluminium in water at elevated temperature

J. G. Auret*, O. F. R. A. Damm*, G. J. Wright* and F. P. A. Robinson†

Cavitation erosion tests were carried out in tap water on aluminium and copper samples in a rotating disk cavitation test apparatus, to study the effect of water temperature on cavitation dynamics and cavitation erosion. A shift in the position of the erosion zone with changing temperature was observed. This was explained in terms of the effect of temperature on the pressure gradient giving rise to cavitation. As had been found for vibratory cavitation, the erosion rate in this case (flow cavitation) increased with increasing water temperature and reached a maximum at approximately 65°C. However, in contrast to copper, which exhibited the usual behaviour, the erosion rate of aluminium did not decrease with further temperature increase. This apparent anomaly was investigated by employing specially developed cells for corrosion rate and temperature measurements on a cavitating aluminium sample. It was found that an increase in corrosion rate was mainly responsible for the high cavitation erosion rate at temperatures above 50°C.

Keywords: *cavitation erosion, elevated temperature, material effects*

Introduction

By definition, cavitation is the phenomenon in which relative movement between a solid object submersed in a liquid and the liquid results in the formation of low-pressure regions in the liquid, leading to localized rapid vaporization. The collapse of these vapour pockets or bubbles takes place extremely rapidly and may lead to damage on nearby solid objects. This form of damage is known as cavitation erosion and is often encountered in hydraulic machinery.

So-called flow-type cavitation erosion is caused by unidirectional relative movement between the liquid and the solid object (e.g. a ship's screw), as opposed to vibratory cavitation erosion. The distinction is purposefully made between these forms of cavitation erosion because of different damage mechanisms[1,2] and a lack of agreement between erosion results[1,3] that have been reported in the literature. It appears that the main differences between vibratory and flow cavitation are associated with the relative importance of rectified diffusion and degasification in fluids experiencing vibratory cavitation[3], as well as different bubble collapse geometries[4,5], leading to results which have proven difficult to explain under certain conditions.

Previous workers ascribed the influence of liquid temperature variation on cavitation erosion to several factors, including: (1) changes in liquid properties, such as viscosity, vapour pressure, surface tension and density, and the effect of these changes on bubble dynamics; (2) changes in dissolved gas content of the fluid; and (3) material property changes[6]. Vibratory test rigs have been mainly used[7–14], although some older work was done in flowing devices of the venturi type[15,16]. The latter results were, however, incomplete and did not allow for final conclusions to be made. Results from vibratory-type rigs with temperatures ranging between the melting and boiling points of several liquids[11] indicated that erosion rate increased slightly with temperature up to a maximum and then decreased considerably (Fig 1). The peak generally occurred about midway between the freezing and the boiling points of the cavitating liquid.

Although controversy exists on the exact cause for the low temperature decrease, Leith[17] argued that the high viscosity and surface tension of the fluid (Fig 2) were responsible for reduction in bubble collapse energy. Other hypotheses put forward were increased gas solubility and bubble collapse cushioning[18,19], inhibition of corrosion[19] and the combined effect of these changes[20].

* *Division of Materials Science and Technology, CSIR, PO Box 395, Pretoria, 0001, South Africa*
† *Professor of Corrosion Science and Engineering, University of Witwatersrand, PO WITS, 2050, South Africa*
Received 3 January 1993; revised 14 May 1993; accepted 30 June 1993

 0301-679X/93/060421-09

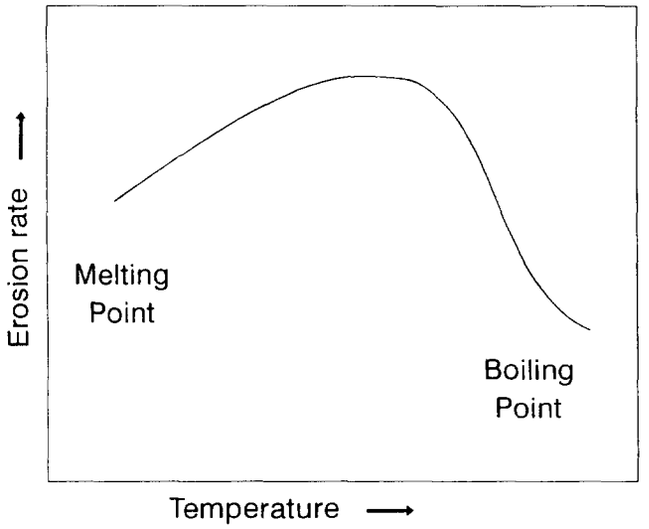

Fig 1 Previous studies[7–14] showed peaking of the erosion rate as a function of temperature, between the melting point and boiling point of the cavitating liquid

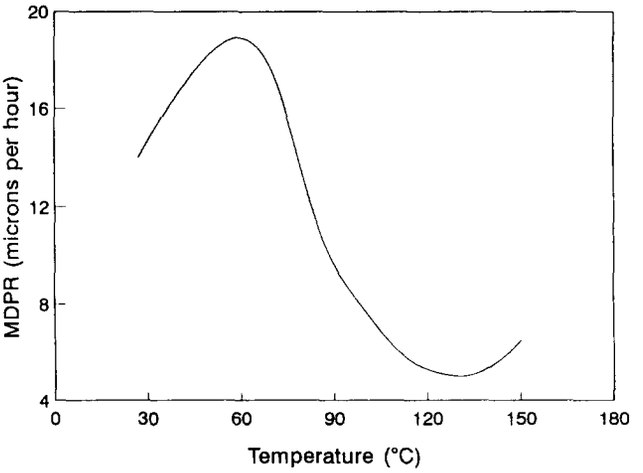

Fig 3 MDPR versus temperature for type 2024 Al alloy tested in a vibratory-type test rig in tap water[21]. MDPR (mean depth of penetration rate) is defined as erosion rate divided by the area being eroded

The damage reduction at elevated temperature was generally associated with the so-called thermodynamic effect[3]. When the local liquid pressure drops sufficiently for cavitation to take place, a cavitating bubble grows by vaporization. In this process latent heat is extracted from the surrounding liquid layer, i.e. the vapour pressure inside the bubble drops, thus retarding bubble growth. Since vapour pressure changes exponentially with temperature (Fig 2), the effect is more pronounced at elevated temperature. An opposing mechanism, namely material weakening and increased corrosion rate as a result of increased temperature, will be most significant in the case of low melting point materials. An example was reported for an aluminium alloy[21] for which a second rise in erosion rate occurred (Fig 3).

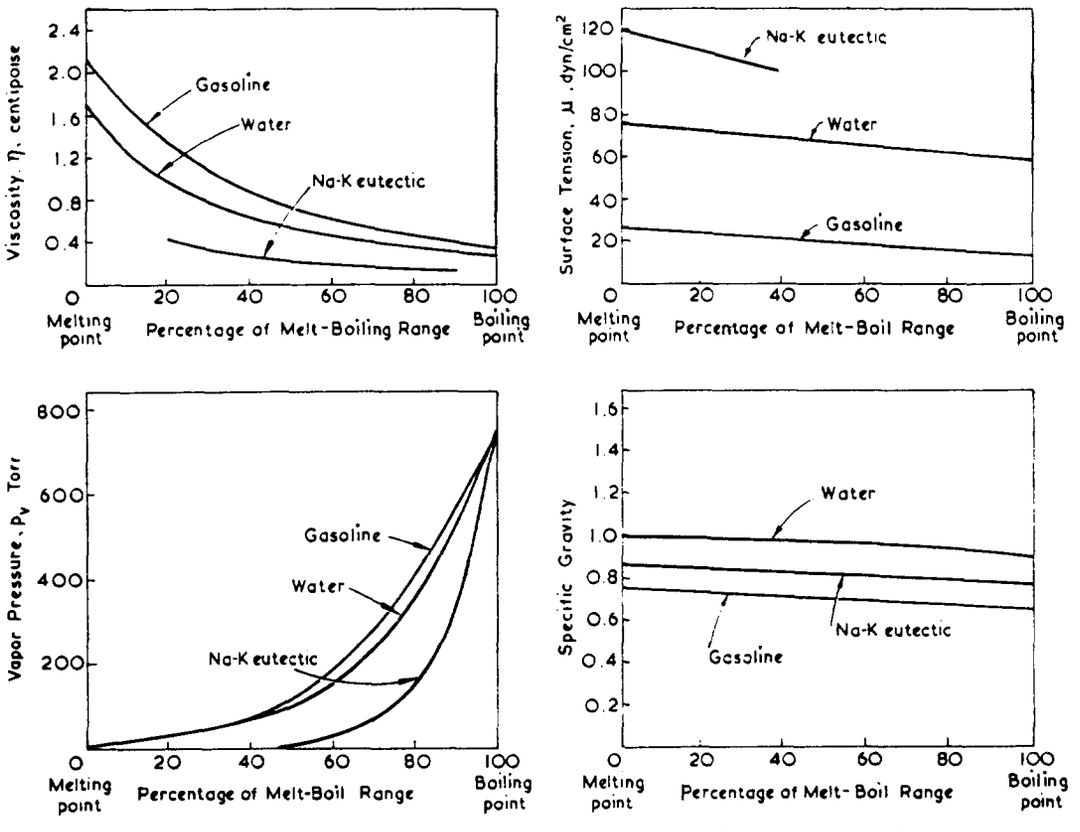

Fig 2 The influence of temperature on the vapour pressure, viscosity, surface tension and specific gravity of water, gasoline and Na–K eutectic mixture[17]

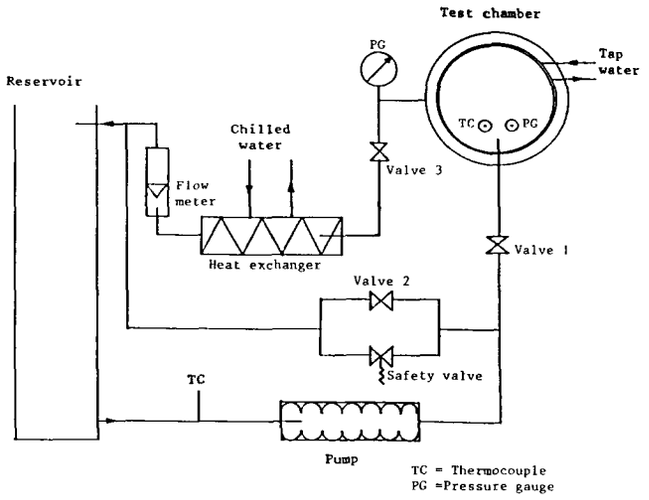

Fig 4 Schematic of cavitation test rig

In the present work, the behaviour of cavitation dynamics and erosion resistance as a function of temperature was studied in tap water for aluminium and copper in a rotating disk cavitation test rig. The unusual temperature dependence of the erosion resistance of aluminium was further elucidated. A relation between cavitation geometry and temperature was also found which had not been reported previously.

Cavitation erosion of aluminium and copper

Procedure for erosion testing

The rotating disk-type test rig shown in Fig 4 was used in the present study. Details of the rig are given elsewhere[22].

Initial erosion testing was carried out on samples made from AA type 1200 aluminium alloy (corresponding to BS 1C and A199,0 in the UK and Germany, respectively) in the H4 annealed condition (Table 1). This material was selected for testing since it erodes easily[23] and has well-known damage mechanisms under cavitation attack[24]. To verify that the apparent anomalies observed in the erosion resistance of the aluminium alloy at high temperatures were material-related, tests were also carried out on commercially pure copper, which has a higher melting point and better resistance to chemical attack.

Test samples were machined to 65 × 24 × 4 mm, after which the surfaces exposed to cavitation were ground and polished to $R_a \sim 0.1$ μm. The samples were stored in a desiccator at all times when not being tested. Three samples, arranged as shown in Fig 5 in the disk, were tested simultaneously. Before and after each test, they were cleaned in ethanol, dried and weighed to the nearest 0.1 of a milligram. The average mass loss, converted to volume loss, was used to determine the erosion rate. Several tests were repeated to verify reproducibility of results.

Two test series were carried out using potable tap water as the test liquid. In the one case, 4-hour tests were started at ambient temperature. In the other case, the test period was 1 hour. To prevent temperature rises during testing, the water was preheated to the test temperature. Although the temperature (and hence air content) control, and thus also the accuracy of the erosion results, for the 1-hour tests was higher than for the 4-hour tests, the observed trends were identical.

Results for cavitation dynamics

An examination of the cavitation cloud (by means of a stroboscope) and the damaged zone on the samples revealed that temperature affected the cavitation geometry. Figure 6 shows the damaged zones on the aluminium samples for various temperatures. The centre of the erosion zone moved further downstream (i.e. away form the inducer hole) as temperature increased. In order to quantify this effect, Fig 7 shows the separation distance between the inducer hole and erosion zone, plotted as a function of temperature. The shape of the erosion zone was fairly constant, except for the growth of the small secondary cavitation zone (caused by the main erosion hole) with increasing temperature.

No previous reference has been found on the effect of temperature on cavitation geometry, although it may give important clues about the changes in bubble dynamics. It has been found in the present study that the temperature dependence of the cavitation-controlling pressure gradient (Fig 8(a)) can be applied to explain the changes in cavitation geometry on a qualitative basis. It is known (Fig 9) that a unique relation exists between nucleus size and vaporization pressure[25]. Consider for the moment the nuclei which vaporize (cavitate) at exactly vapour pressure, P_v. Since P_v increases with temperature (Fig 2), these

Table 1 Composition and typical mechanical properties of AA type 1200 Al alloy, H4[a] annealed condition

Chemical composition									Mechanical properties		
Al (min)	Cu	Mg	Si	Fe	Mn	Zn	Ti	Cr	0.2% PS (MPa)	TS (MPa)	% el in 50 mm
99.0	0.05	–	Fe + Si 1.0		0.05	0.1	0.05	–	105	125	8

[a]*Strain hardened. Material subjected to the application of cold work after annealing (or hot forming), or to a combination of cold work and partial annealing/stabilizing in order to secure the specified mechanical properties. H2, H4, H6, etc. indicate ascending order of tensile strength*

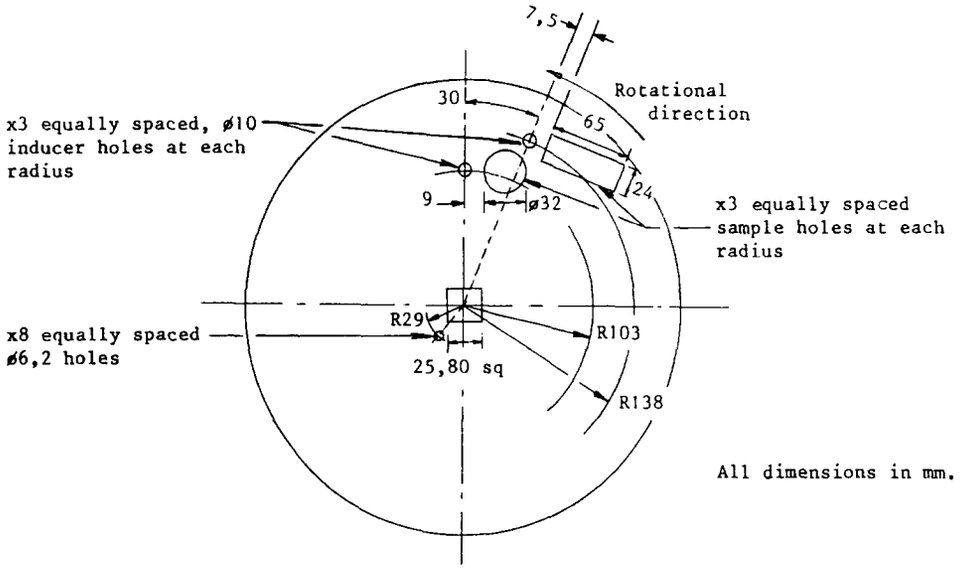

Fig 5 Disk design allowing for three rectangular or three round samples

Fig 6 Type 1200 Al alloy samples eroded for 1 hour at 44.8; 49.8; 65.5 and 78.8°C from top to bottom. The inducer holes were located on the left

nuclei will start vaporizing earlier at a higher temperature, i.e. a shorter distance downstream of the inducer hole as shown in Fig 8(b). For the same reason, condensation will occur further downstream than at lower temperature. Thus the cavitation cloud will

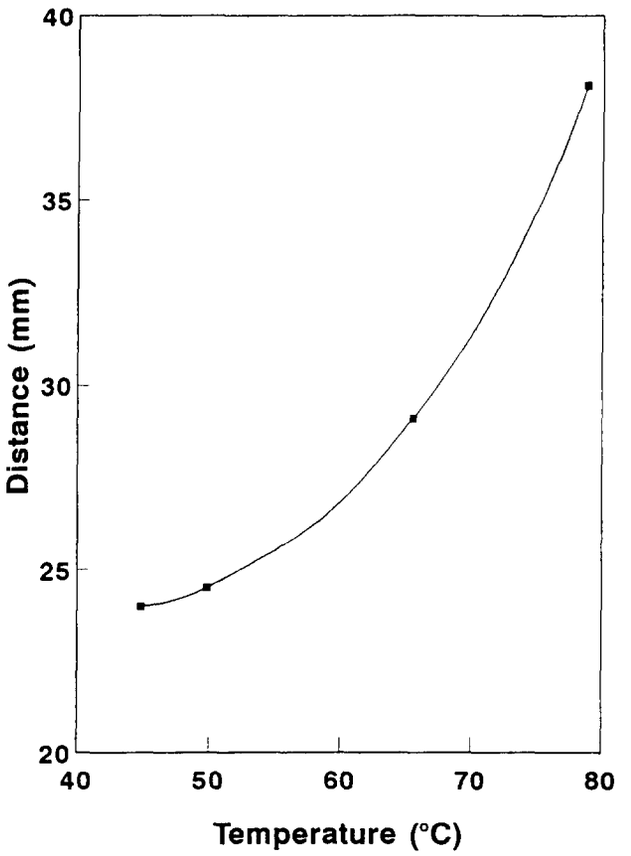

Fig 7 The distance between the downstream edge of the inducer hole and the centre of the main erosion zone, plotted as a function of temperature for the 1-hour tests

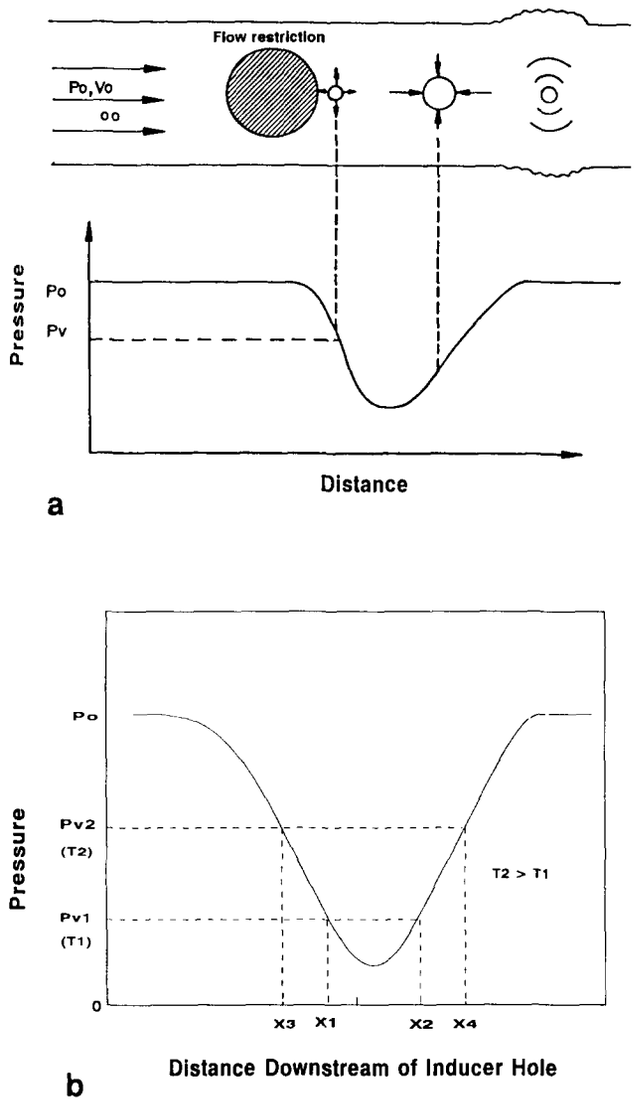

Fig 8 (a) Hypothetical presentation of the pressure profile associated with flow cavitation and (b) the effect of temperature on bubble dynamics. Nuclei extend their travelling distance in the pressure interval below P_v *from* x_1x_2 *at temperature* T_1 *to* x_3x_4 *at* T_2

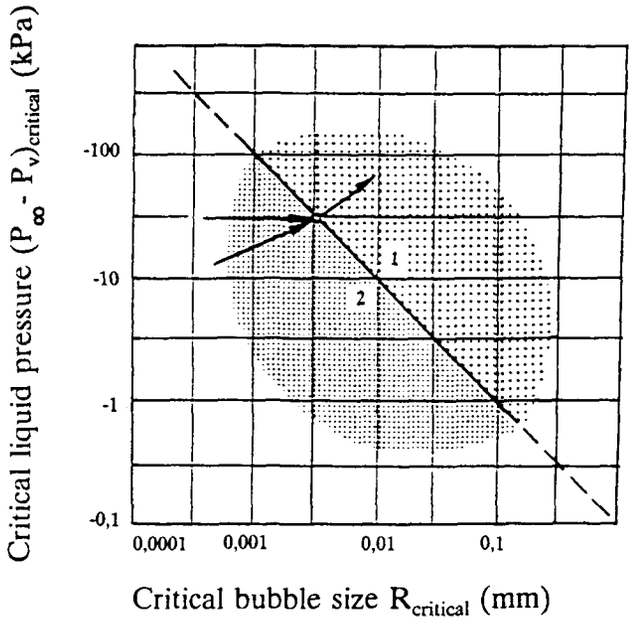

Fig 9 Critical size of cavitation nuclei at 20°C[25]. The bubbles must grow up to the boundary curve before vaporization commences

grow in the downstream direction with increasing temperature. (The upstream end already extends up to the inducer hole in this particular case.) As a result, the erosion zone which coincides approximately with the downstream end of the fixed cavity[23] will also move downstream.

Erosion results

The test parameter values listed in Table 2 were used for the tests. Erosion data are plotted in Fig 10.

The 1-hour volume loss against a temperature graph for aluminium showed that the peak volume loss for aluminium occurred already at approximately 65°C, but that no significant decrease followed at higher temperatures; in fact, the graph flattened out. This result was not in line with the usual trend and indicated that the role of material weakening and increased corrosion rate[21] needed further elucidation. Visual examination of samples revealed that those tested at 80°C exhibited a shiny appearance. Scanning electron microscope (SEM) examination of sample surfaces showed increased corrosion activity both inside (Fig 11(a)) and outside (Fig 11(b)) the erosion zone of samples tested at 80°C, as opposed to 50°C (Fig 12). It appeared that material was corroded away around second-phase particles found by energy-dispersive X-ray analysis (EXD) to consist mainly of Al and Fe. The composition of these particles is typically Al_6Fe or Al_3Fe[26], both of which are cathodic to the aluminium solid solution matrix[27]. As a result, corrosion will progress more rapidly in the solid solution immediately surrounding the particles.

As discussed earlier, commercially pure copper was then included in the test programme to verify whether or not the results obtained for aluminium were material-specific. As illustrated in Fig 10, the volume loss for copper decreased drastically above 50°C. This is in agreement with the 'normal' reported trend.

It would thus appear that the erosion behaviour of copper as a function of temperature is governed by the same phenomena (thermodynamic effects, viscosity and surface tension variations, etc.) identified previously for vibratory tests. However, in the case of aluminium, inverse material effects seem to override these phenomena at elevated temperature. To clarify this issue, the influence of increased temperatures on the corrosion resistance and mechanical strength of aluminium has been investigated, as described below.

Table 2 Fluid and flow parameter values for (a) the 4-hour and (b) the 1-hour temperature tests

(a)

Parameter	Mean value	Standard deviation	Comment
Pressure (MPa)	0.14	0.002	
Dissolved oxygen content (mg/ℓ)	7.50	0.71	No direct control. Max. operating temperature 60°C, so no measurements could be taken for tests above this temperature
Disk velocity (rpm)	3521	24	
Flow rate (ℓ/min)	~ 30		

(b)

Parameter	Mean value	Standard deviation	Comment
Pressure (MPa)	0.15	0.02	
Dissolved oxygen content (mg/ℓ)	6.69	0.45	No direct control. Max. temperature is 60°C
Disk velocity (rpm)	3629	14	
Flow rate (ℓ/min)	~ 30		

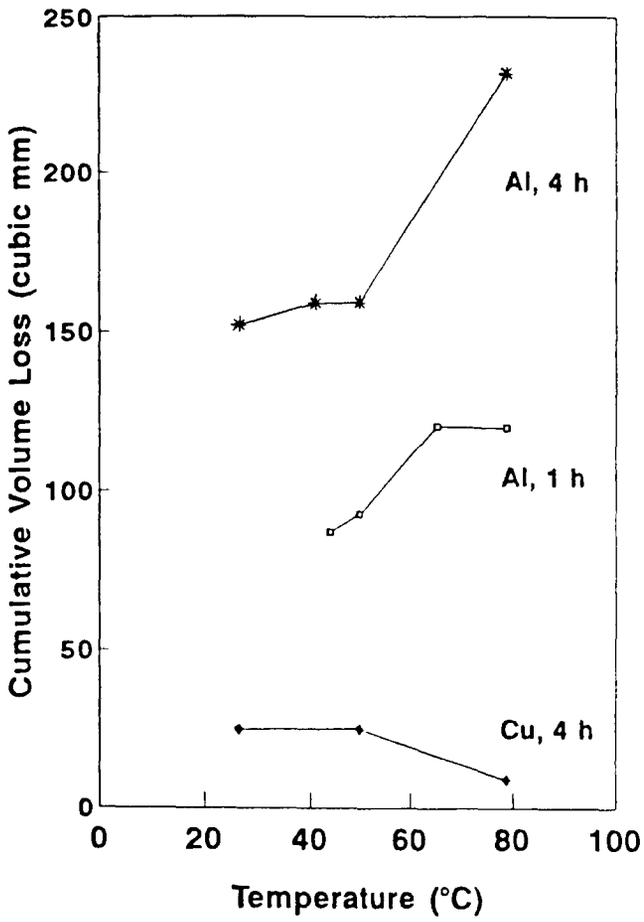

Fig 10 Effect of temperature for the 4-hour and 1-hour erosion tests

Temperature-related material effects on aluminium

Corrosion

It is well known that cavitation and corrosion, when acting simultaneously, will produce far more damage than just the sum of the two separate effects[28–33]. By implication, a relatively small increase in corrosion rate of a sample may thus have a substantial effect on volume loss.

In order to measure the influence of corrosion at elevated temperature on the erosion rate of type 1200 Al alloy, a special disk-and-sample arrangement employing the same disk and sample geometry as in Fig 5 was tested in the rotating disk test rig. The arrangement, illustrated in Fig 13, comprised an aluminium disk with a radial slot connecting the sample recess and the hollow drive shaft. A corrosion cell was constructed consisting of a 6 mm diameter sample electrode made from type 1200 Al alloy, a stainless steel auxiliary electrode and a stainless steel reference electrode. The electrodes were cast in an epoxy into a stainless steel frame. After setting, the exposed cell face was ground and polished flat and the cell was fitted into the sample recess in the disk. The electrode wires were passed along the radial slot in the disk and through the hollow centre of the drive shaft, which was subsequently sealed with epoxy. The wires were then connected via a slipring assembly to a potentiostat.

The test parameters are listed in Table 3. Corrosion rates were measured using the linear polarization resistance (LPR) technique. Temperatures were 50°C, 60°C and 80°C, while three erosion conditions were employed: disk *stationary* (S); disk *rotating* with no cavitation, achieved by filling up the inducer holes (R); and disk rotating with normal *cavitation* (C).

Results are shown in Fig 14. Important observations are:

- At 50°C the corrosion rate is higher with the disk rotating than with it stationary. This is due to the improved supply of oxygen to the corroding surface, and thus an increased reaction rate, when the disk is rotating. The reversal of this trend at 80°C may be explained in terms of the change in corrosion mode, i.e. the formation of pits at this temperature (see Fig 11). The rotational motion reduces the acidification of the pit contents; therefore the corrosion rate is lower than with the disk stationary.
- At any particular temperature, the corrosion rate is higher for cavitating as opposed to stationary or

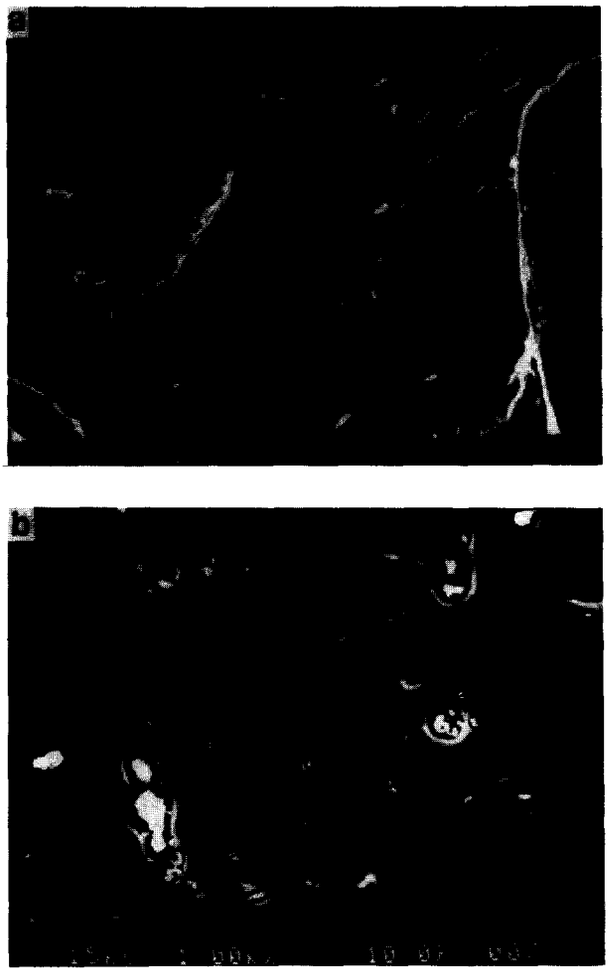

Fig 11 SEM micrographs of sample surfaces corroded at 80°C, taken (a) within and (b) outside the erosion zone (10 mm = 13.3 μm)

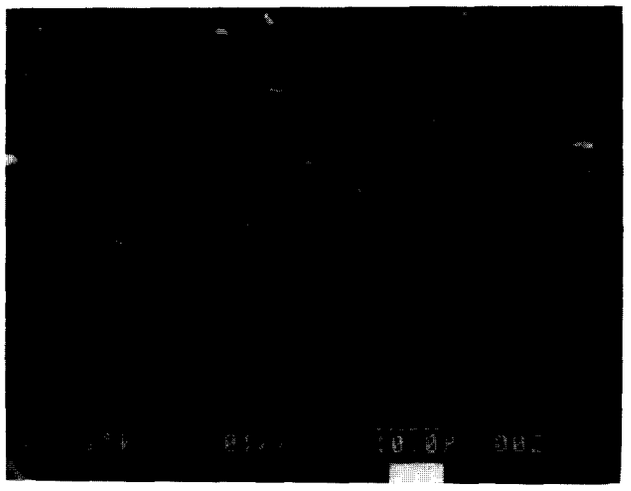

Fig 12 SEM micrograph of samples surface eroded at 50°C, outside erosion zone (10 mm = 13.3μm)

rotating-only conditions. This demonstrates clearly the synergism between cavitation erosion and corrosion.

- With increasing temperature, the corrosion rate under cavitating conditions becomes higher, i.e. corrosion damage will increase with temperature.

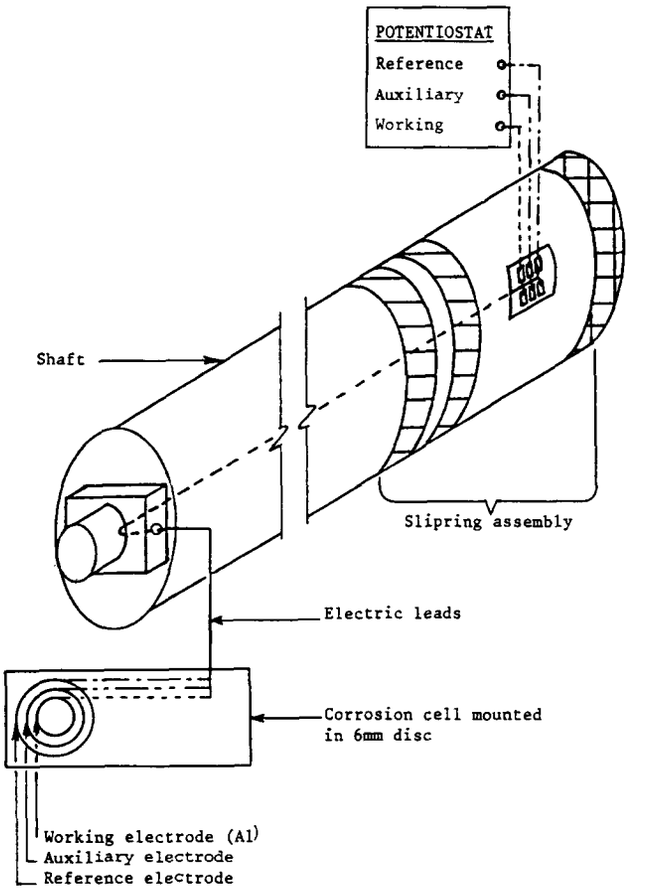

Fig 13 Measuring system to investigate the corrosion behaviour of type 1200 Al alloy in the rotating disk rig

Table 3 Test parameters for corrosion rate measurements

Test fluid	Tap water
Temperature (°C):	
(i) mean	50; 60; 80
(ii) range	1
Static presure (MPa):	
(i) mean	0.15
(ii) range	0.01
Flow rate (ℓ/min)	~30
Disk velocity (rpm)	~3600

Mechanical degradation

Measurements made by embedded thermocouples during tests over a range of water temperatures showed that the local specimen temperature within the eroded area was never significantly different from that outside this area, and both areas were slightly cooler than the surrounding water. Similar observations have been made by Singer and Harvey[35], and suggest that the local temperatures were not high enough to cause a significant decrease in mechanical strength.

Conclusions

Using a rotating disk test rig, type 1200 Al alloy showed no substantial drop in erosion rate in tap

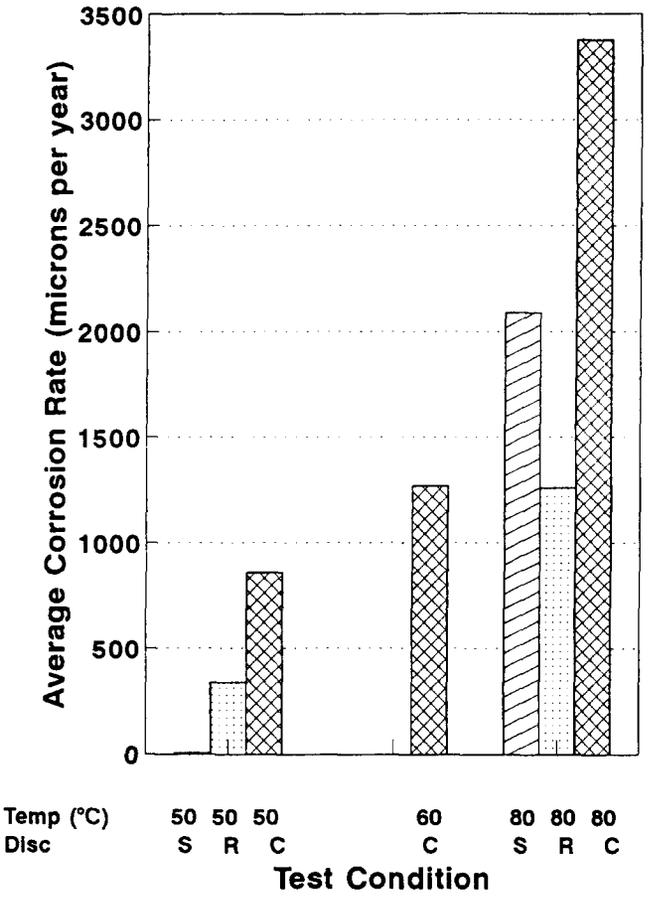

Fig 14 Bar chart showing the influence of cavitation and temperature on the corrosion rate of type 1200 Al alloy

water at elevated temperatures. As inferred in the literature and confirmed with erosion tests on copper, thermodynamic effects lead to a decrease in cavitation erosion damage at temperatures approaching the boiling point of the cavitating liquid. The high damage rate on aluminium may thus be ascribed to material-related factors, such as increased corrosion rate and mechanical weakening, which oppose the thermodynamic effects. Corrosion rate and temperature measurements on cavitating cells in the rotating disk rig showed that the major contribution to the increased damage suffered by type 1200 Al alloy arose from an increase in the corrosion rate.

References

1. **Karimi A. and Martin J.L.** Cavitation erosion of materials. *Int. Met. Rev. 1986* **31**(1), 1–26
2. **Preece C.M. and Brunton J.H.** A comparison of liquid impact erosion and cavitation erosion. *Wear 1980*, **60**, 269–284
3. **Hammitt F.G.** *Cavitation and Multiphase Flow Phenomena*, McGraw-Hill, New York, 1980
4. **Hansson I., Mørch K.A. and Preece C.M.** A comparison of ultrasonically generated cavitation erosion and natural flow cavitation erosion. In: *Ultrasonics International*, IPC Science and Technology Press Ltd, Guildford, UK, 1978, pp. 267–272
5. **Hansson I. and Mørch K.A.** Comparison of the initial stage of vibratory and flow cavitation erosion. *Proc. 5th Int. Conf. on Erosion by Solid and Liquid Impact, 1979*, Royal Aircraft Establishment, Farnborough, UK, pp. 60-1–60-9
6. **Preece C.M.** Cavitation erosion. In: *Treatise on Matls. Sci. Tech.* **16**, 1979, pp. 249–308
7. **Hobbs J.M. and Laird A.** Pressure, temperature and gas content effects in the vibratory test. *NEL Report 438*, October 1969
8. **Young S.G. and Johnston J.R.** Effect of cover gas pressures on accelerated damage in sodium. *NASA TN D-4235*, November 1967
9. **Young S.G. and Johnston J.R.** Accelerated cavitation damage of steels and superalloys in liquid metals. *NASA TN D-3226*, May 1966
10. **Hammitt F.G. and Rogers D.O.** Effect of pressure and temperature variation in vibratory cavitation damage test. *J. Mech. Engr. Sci. 1970*, **12**(6), 432–439
11. **Hammitt F.G. and Bhatt N.R.** Cavitation damage at elevated temperature and pressure. *ASME Cavitation and Polyphase Flow Forum*, 1972, pp 11–13
12. **Garcia R. and Hammitt F.G.** Cavitation damage and correlation with material and fluid properties. *Trans. ASME, J. Basic Engr., Ser. D. 1967*, **89**(4), 753–763
13. **Devine R.E. and Plesset M.S.** Temperature effects in cavitation damage. *CIT Rept 85-27*, Pasadena, California, April 1964
14. **Hammitt F.G. and Bhatt N.R.** Temperature and pressure effects in vibratory cavitation damage tests in various liquids, including molten sodium. *Proc. 5th Conf. on Fluid Machinery*, 1975, Akademia Kiado, Budapest, Hungary, pp. 393–402
15. **Mousson J.M.** Pitting resistance of metals under cavitating conditions. *Trans. ASEM 1937*, **59**, 399–408
16. **Shal'nev K.K., Varga J.J. and Sebestyen G.** Scale-effect investigation of cavitation erosion using the energy parameter. In: *Erosion by Cavitation or Impingement* ASTM STP 408, 1967, p. 220
17. **Leith W.C.** Prediction of cavitation damage in the alkali liquid metals. *Proc. Am. Soc. Test. Mater. 1965*, **65**, 789–800
18. **Eisenberg P.** On the mechanisms and prevention of cavitation. *David Taylor Model Basin Rept No. 712*, Washington, 1950
19. **Plesset M.S.** Temperature effects in cavitation damage. *Trans. ASME J. Basic Engr., Ser. D 1972*, **94**, 559–566
20. **Heathcock C.J.** *Cavitation erosion of materials*, PhD thesis, Materials Engineering Dept, University of Cape Town, 1980
21. **Wang X., Zhou Y. and Hammitt F.G.** Vibratory cavitation erosion tests at 120–150°C and 2 bar suppression pressure. *ASME Cavitation and Multiphase Flow Forum, 1984*
22. **Auret J.G. *et al.*** A simple model for the pressure and velocity dependence of flow-type cavitation erosion. *Wear*, submitted for publication
23. **Knapp R.T., Daily J.W. and Hammitt F.G.** *Cavitation*, McGraw-Hill, New York, 1970
24. **Vyas B. and Preece C.M.** Cavitation-induced deformation of aluminium. *ASTM STP 567*, 1974, pp. 77–105
25. **Daily J.W. and Johnson V.E.** Turbulence and boundary layer effects on cavitation inception from gas nuclei. *Trans. ASME*, November 1956
26. **Hatch J.E.** (Ed.) *Aluminium: Properties and Physical Metallurgy*, ASM, 1984, p. 60
27. **Mears R.B. and Brown R.H.** Causes of corrosion currents. *Ind. Eng. Chem. 1941*, **33**, 1001
28. **Petracchi G.** Investigation of cavitation corrosion (in Italian). *Metallurgica Italiana 1944*, **41**, 1–6; English summary in *Engr's Digest 1949*, **10**, 314–316
29. **Plesset M.S.** Cathodic protection in cavitation damage. *Trans. ASME, J. Basic Engr., Ser. D. 1960*, **82**, 808–820
30. **Leith W.C. and Thompson A.L.** Some corrosion effects in accelerated cavitation damage. *Trans. ASME, J. Basic Engr., D 1960*, **82**, 795–807
31. **Preece C.M.** Erosion of metals and alloys. In: *Surface Effects in Crystal Plasticity*, Latanision R.M. and Fourie J.T. (Eds). Noordhoff, Leyden, 1977

32. **Evans U.R.** *The Corrosion and Oxidation of Metals*, Edward Arnold, London, 1960

33. **Hoar T.P. and Scully J.C.** Mechanochemical anodic dissolution of austenitic stainless steel in hot chloride solution at controlled electrode potential. *J. Electrochem. Soc. 1964*, **111**, 348–352

34. Properties and selection: nonferrous alloys and pure metals. In: *Metals Handbook* 9th edition, **2**, ASM, 1979

35. **Singer B.G. and Harvey S.J.** Gas content and temperature effects in vibratory cavitation tests. *Wear 1979*, **52,** 147–160